




Article

Regulation of CIC-2 Chloride Channel Proteostasis by Molecular Chaperones: Correction of Leukodystrophy-Associated Defect

Ssu-Ju Fu ^{1,2}, Meng-Chun Hu ¹, Cheng-Tsung Hsiao ^{1,3}, An-Ting Cheng ¹, Tsung-Yu Chen ⁴, Chung-Juan Jeng ^{2,5,*} and Chih-Yung Tang ^{1,6,*} 

¹ Department of Physiology, College of Medicine, National Taiwan University, Taipei 10051, Taiwan; d01441001@ntu.edu.tw (S.-J.F.); mengchun@ntu.edu.tw (M.-C.H.); hsiaoct26@gmail.com (C.-T.H.); r08441010@ntu.edu.tw (A.-T.C.)

² Institute of Anatomy and Cell Biology, College of Medicine, National Yang Ming Chiao Tung University, Taipei 12212, Taiwan

³ Department of Neurology, Taipei Veterans General Hospital, Taipei 12217, Taiwan

⁴ Center for Neuroscience and Department of Neurology, University of California, Davis, CA 95616, USA; tycchen@ucdavis.edu

⁵ Brain Research Center, National Yang Ming Chiao Tung University, Taipei 12212, Taiwan

⁶ Graduate Institute of Brain and Mind Sciences, College of Medicine, National Taiwan University, Taipei 10051, Taiwan

* Correspondence: cjeng@ncyu.edu.tw (C.-J.J.); tang@ntu.edu.tw (C.-Y.T.)



Citation: Fu, S.-J.; Hu, M.-C.; Hsiao, C.-T.; Cheng, A.-T.; Chen, T.-Y.; Jeng, C.-J.; Tang, C.-Y. Regulation of CIC-2 Chloride Channel Proteostasis by Molecular Chaperones: Correction of Leukodystrophy-Associated Defect. *Int. J. Mol. Sci.* **2021**, *22*, 5859.

<https://doi.org/10.3390/ijms22115859>

Academic Editor: Nikolas Nikolaidis

Received: 30 March 2021

Accepted: 26 May 2021

Published: 30 May 2021

Publisher's Note: MDPI stays neutral with regard to jurisdictional claims in published maps and institutional affiliations.



Copyright: © 2021 by the authors. Licensee MDPI, Basel, Switzerland. This article is an open access article distributed under the terms and conditions of the Creative Commons Attribution (CC BY) license (<https://creativecommons.org/licenses/by/4.0/>).

Abstract: The CIC-2 channel plays a critical role in maintaining ion homeostasis in the brain and the testis. Loss-of-function mutations in the CIC-2-encoding human *CLCN2* gene are linked to the white matter disease leukodystrophy. *Clcn2*-deficient mice display neuronal myelin vacuolation and testicular degeneration. Leukodystrophy-causing CIC-2 mutant channels are associated with anomalous proteostasis manifesting enhanced endoplasmic reticulum (ER)-associated degradation. The molecular nature of the ER quality control system for CIC-2 protein remains elusive. In mouse testicular tissues and Leydig cells, we demonstrated that endogenous CIC-2 co-existed in the same protein complex with the molecular chaperones heat shock protein 90 β (Hsp90 β) and heat shock cognate protein (Hsc70), as well as the associated co-chaperones Hsp70/Hsp90 organizing protein (HOP), activator of Hsp90 ATPase homolog 1 (Aha1), and FK506-binding protein 8 (FKBP8). Further biochemical analyses revealed that the Hsp90 β -Hsc70 chaperone/co-chaperone system promoted mouse and human CIC-2 protein biogenesis. FKBP8 additionally facilitated membrane trafficking of CIC-2 channels. Interestingly, treatment with the Hsp90-targeting small molecule 17-allylamino-17-demethoxygeldanamycin (17-AAG) substantially boosted CIC-2 protein expression. Also, 17-AAG effectively increased both total and cell surface protein levels of leukodystrophy-causing loss-of-function CIC-2 mutant channels. Our findings highlight the therapeutic potential of 17-AAG in correcting anomalous CIC-2 proteostasis associated with leukodystrophy.

Keywords: proteostasis; channelopathy; protein quality control; chaperone; co-chaperone; 17-AAG

1. Introduction

The ubiquitously expressed CIC-2 chloride (Cl⁻) channel is activated by membrane hyperpolarization and osmotic cell swelling, and plays an essential role in the regulation of Cl⁻ homeostasis in a wide variety of different tissues [1–7]. In mice, knockout of the *Clcn2* gene, which encodes the voltage-gated CIC-2 channel, results in neuronal fluid accumulation and myelin vacuolation in the brain, as well as substantial degeneration of the retina and the testis [8–10]. In humans, loss-of-function mutations in the *CLCN2* gene are associated with a subtype of the white matter disorder leukodystrophy, also known as *CLCN2*-related leukoencephalopathy, manifesting as intramyelinic edema in the brain and

perhaps infertility [11–14]. Along with other studies in different types of *Clcn2*-deficient mice [15,16], these findings support the notion that the CIC-2 channel is important for extracellular ion homeostasis in the brain and the testis.

Patients with *CLCN2*-related leukoencephalopathy present with homozygous or compound-heterozygous mutations, indicating that this rare disorder is primarily caused by autosomal recessive mutations in the *CLCN2* gene [11,12,14,17–19]. To date, more than 10 disease-related *CLCN2* mutations have been identified, including missense, insertion, and deletion mutations. Functional and biochemical analyses show that, in addition to altered voltage-dependent gating property and reduced Cl^- current amplitude, leukodystrophy-causing CIC-2 mutant channels are associated with defective protein stability and impaired membrane trafficking [11,13,20], consistent with the presence of disease-related anomalous CIC-2 protein homeostasis (proteostasis). Proteostasis is largely maintained by multiple translational and post-translational mechanisms, thereby ensuring appropriate conformation, stability, and subcellular localization of proteins [21,22]. One of the crucial proteostasis mechanisms for membrane proteins entails selective removal of misfolded proteins from the endoplasmic reticulum (ER) and subsequent degradation by the proteasome, commonly referred to as ER-associated degradation [23,24].

ER-associated degradation comprises a series of stringent protein quality control systems, as well as concerted activity of ubiquitination machinery [24–26]. Elucidation of the interplay between CIC-2-related ER protein quality control systems and proteasomal degradation pathways is therefore essential for addressing the molecular pathophysiology of leukodystrophy. We demonstrated recently that the cullin 4 (CUL4)-damage-specific DNA binding protein 1 (DDB1)-cereblon (CRBN) E3 ubiquitin ligase complex promotes ubiquitination and ER-associated degradation of wild-type (WT) and disease-related mutant CIC-2 channels [20]. The molecular nature of the ER quality control system for CIC-2 protein, however, is still unclear.

A cardinal process during ER protein quality control involves conformation surveillance of nascent polypeptides by a network of molecular chaperones and cofactors (co-chaperones) that proficiently facilitate protein folding, thereby minimizing degradation of misfolded proteins [27–29]. Interestingly, the interconnected heat shock protein 70 (Hsp70) and heat shock protein 90 (Hsp90) molecular chaperone systems, along with their associated co-chaperones such as Hsp70/Hsp90 organizing protein (HOP), activator of Hsp90 ATPase homolog 1 (Aha1), and FK506-binding protein 8 (FKBP8), have been demonstrated to play essential roles in ER quality control of several types of Cl^- channels [30–34]. In the current study, we set out to identify the chaperone/co-chaperone network monitoring endogenous CIC-2 proteostasis in mouse testicular tissues and Leydig cells. By employing heterologous expression in the human embryonic kidney (HEK) 293T cells, we also explored the therapeutic potential of correcting leukodystrophy-associated anomalous human CIC-2 proteostasis by modulating chaperone/co-chaperone activity.

2. Results

2.1. Association of Endogenous CIC-2 with Chaperones and Co-Chaperones in Native Tissue

Previous biochemical evidence supports the interaction between the CIC-2 Cl^- channel and the molecular chaperone Hsp90 in the mouse brain [35]. We therefore began by asking whether this well-known molecular chaperone, as well as its associated molecular chaperone and co-chaperones, may interact with endogenous CIC-2 protein profusely expressed in mouse testes (Figure 1A). Consistent with the previous observation in the mouse brain, Figure 1B depicts that endogenous CIC-2 in testes was readily co-immunoprecipitated with Hsp90 β , the constitutive Hsp90 isoform. Furthermore, the molecular chaperone heat shock cognate protein 70 (Hsc70), the constitutively expressed Hsp70 isoform, also co-existed in the same protein complex with endogenous CIC-2 (Figure 1C). Our co-immunoprecipitation study further identified HOP, a soluble co-chaperone regulating Hsp90 ATPase activity and mediating the interaction of Hsp70 and Hsp90 [27,36], as a binding partner of endogenous CIC-2 (Figure 1D). Figure 1E illustrates that Aha1, another cytosolic co-chaperone

regulating the ATPase activity of Hsp90 [27,36], was also co-immunoprecipitated with endogenous CIC-2. Lastly, the co-immunoprecipitation result in Figure 1F is consistent with the idea that endogenous CIC-2 is associated with the co-chaperone FKBP8 (also known as FKBP38), which is an Hsp90-associated membrane-anchored immunophilin with potential peptidyl-prolyl *cis-trans* isomerase function [37,38].

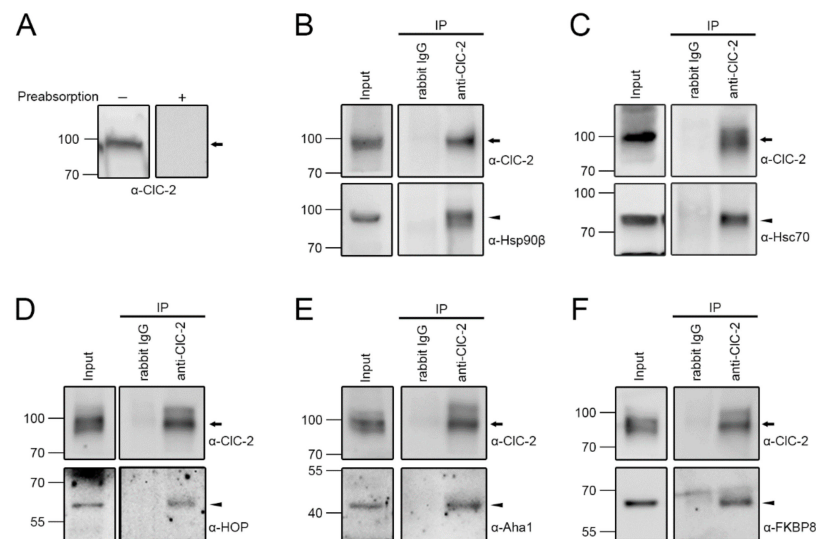


Figure 1. Interaction of molecular chaperones and co-chaperones with endogenous CIC-2 in mouse testes. (A) Endogenous CIC-2 protein signal in mouse testes. The specificity of the rabbit-derived anti-CIC-2 antibody (α -CIC-2) was verified by preabsorption with a control antigen peptide. (B–F) Co-immunoprecipitation of endogenous Hsp90 β (B), Hsc70 (C), HOP (D), Aha1 (E), or FKBP8 (F) with CIC-2. Mouse testis lysates were immunoprecipitated (IP) with the rabbit IgG or α -CIC-2. The molecular weight markers (in kilodaltons) and immunoblotting antibodies (α -Hsp90 β , α -Hsc70, α -HOP, α -Aha1, and α -FKBP8) are labeled to the left and right, respectively. The protein bands corresponding to endogenous CIC-2 and chaperones/co-chaperones are highlighted with the black arrow and the black arrowhead, respectively. Corresponding expression levels of CIC-2 and chaperones/co-chaperones in the lysates are shown in the Input lane. In all cases hereafter, input represents about 10% of the total protein used for immunoprecipitation.

Given that complete knockout of CIC-2 in mice leads to severe testicular degeneration involving abnormal Sertoli cells and hyperplasia of Leydig cells [8,9], we went on to examine the subcellular localization of endogenous CIC-2 and the foregoing chaperones/co-chaperones in a cell line derived from mouse Leydig cells, the MA-10 cell [39,40]. Endogenous CIC-2 protein expression was verified with shRNA knock-down of mouse CIC-2 in MA-10 cells (Figure 2A). As illustrated in Figure 2B, immunofluorescence analyses showed that endogenous CIC-2 channels in MA-10 Leydig cells were abundantly present at the plasma membrane; notably, a prominent portion of endogenous CIC-2 was also present in the perinuclear region and partially co-localized with Hsp90 β . Similarly, a notable fraction of cytoplasmic CIC-2 co-localized with endogenous Hsc70, HOP, Aha1, or FKBP8 in MA-10 cells as well (Figure 2C–F). Taken together, both our biochemical and immunofluorescence data support the notion that endogenous CIC-2 channels are associated with the molecular chaperones Hsp90 β and Hsc70, as well as their co-chaperones HOP, Aha1, and FKBP8.

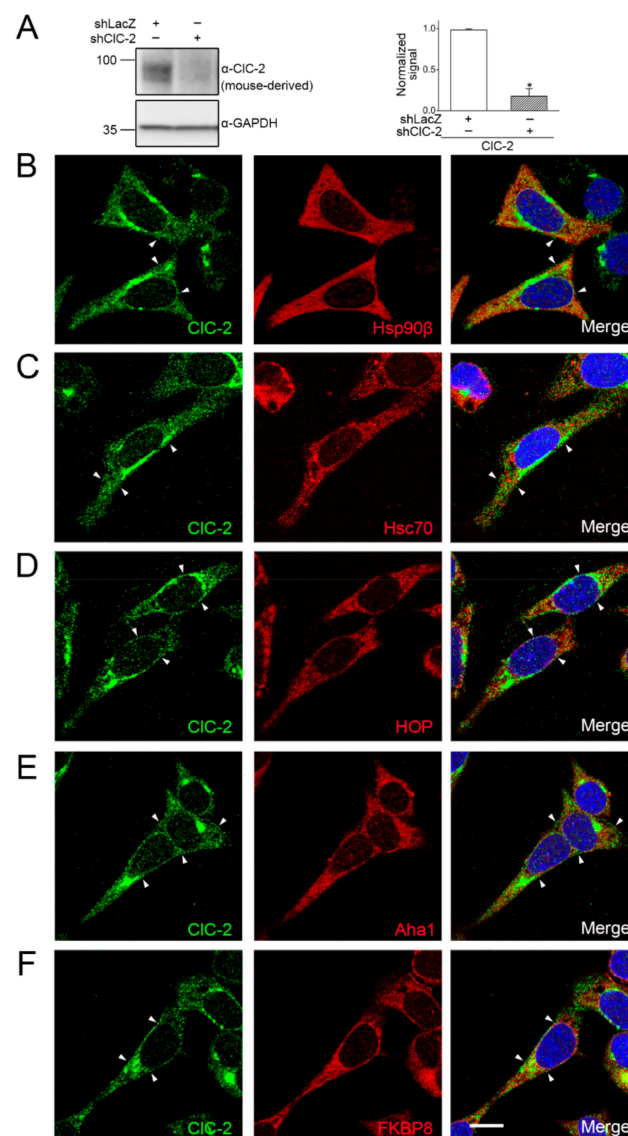


Figure 2. Co-localization of molecular chaperones and co-chaperones with endogenous CIC-2 in mouse MA-10 cells. (A) (Left) Endogenous CIC-2 protein signal in mouse MA-10 Leydig cells. The specificity of the mouse-derived anti-CIC-2 antibody was verified by shRNA knock-down of mouse CIC-2 (shCIC-2). shRNA knock-down of LacZ (shLacZ) was employed as the control experiment. GAPDH was used as the loading control. (Right) Quantification of relative CIC-2 protein levels. Protein density was standardized as the ratio of the CIC-2 signal to the cognate GAPDH signal. Values from the shCIC-2 group (hatched bar) was then normalized to those for the corresponding shLacZ control (clear bar). Asterisk denotes significant difference from the shLacZ control (*, *t* test: $p < 0.05$; $n = 4$). (B–F) Representative confocal micrographs showing the immunofluorescence staining patterns of endogenous CIC-2 (green) and chaperones/co-chaperones (red). Fixed MA-10 cells were stained with the mouse-derived anti-CIC-2 antibody, as well as rabbit-derived antibodies against the indicated molecular chaperones/co-chaperones, under the permeabilized configuration. Merged images of CIC-2 and chaperone/co-chaperone signals are shown in the rightmost panels, where DAPI (blue) was employed as a nuclear counterstain. Arrowheads denote plasma membrane-localization of CIC-2. Scale bar = 15 μ m. Data are representative of at least three independent experiments.

2.2. Regulation of CIC-2 Protein Expression by Chaperones and Co-Chaperones

The next question we asked was whether these molecular chaperones and co-chaperones play a role in endogenous CIC-2 protein expression. To this end, we first employed RNA interference with specific shRNA for various chaperones/co-chaperones in mouse MA-10

Leydig cells. The specificity of the rabbit-derived anti-CIC-2 antibody was verified with shRNA knock-down of mouse CIC-2 in MA-10 cells (Figure 3A). Consistent with a regulatory role of Hsp90 β , shRNA knock-down of endogenous Hsp90 β substantially reduced CIC-2 protein expression in MA-10 cells (Figure 3B). Figure 3C–F further demonstrate that shRNA knock-down of endogenous Hsc70, HOP, Aha1, or FKBP8 decreased CIC-2 protein expression by about 20–36% in MA-10 cells.

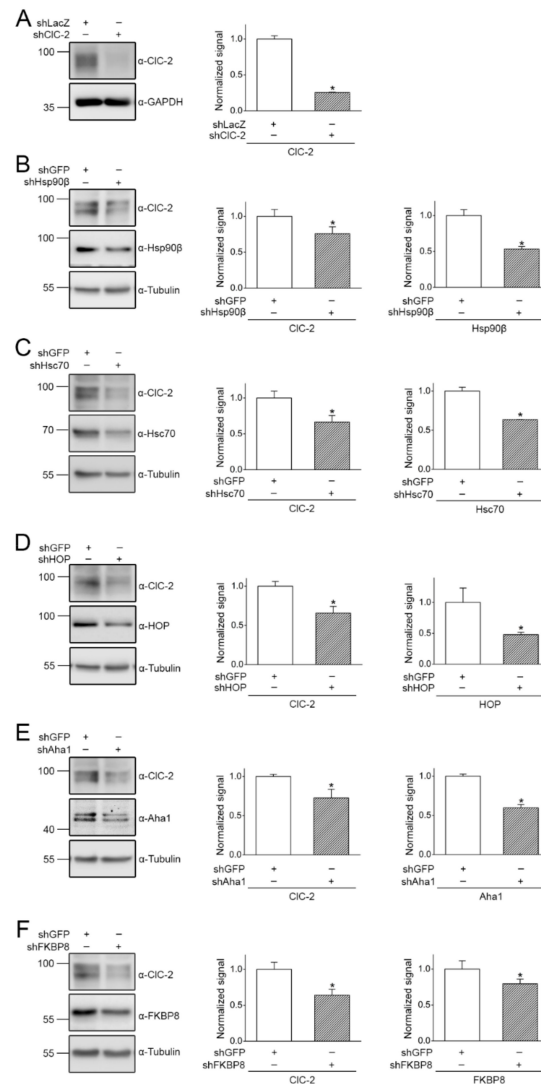


Figure 3. shRNA knock-down of endogenous chaperones or co-chaperones in mouse MA-10 cells. (A) Verification of the specificity of the rabbit-derived anti-CIC-2 antibody in mouse MA-10 Leydig cells. (Left) Representative immunoblot showing the effect of shLacZ and shCIC-2 knock-down on endogenous CIC-2 protein signal. (Right) Quantification of relative CIC-2 protein levels. Protein density was standardized as the ratio of the CIC-2 signal to the cognate GAPDH signal. Values from the shCIC-2 group (hatched bar) was then normalized to those for the corresponding shLacZ control (clear bar). Asterisk denotes significant difference from the shLacZ control (*, *t* test: $p < 0.05$; $n = 3$). (B–F) (Left panels) Representative immunoblots showing the effect of shRNA knock-down of chaperones/co-chaperones (shHsp90 β , shHsc70, shHOP, shAha1, and shFKBP8) on endogenous CIC-2 expression. Infection with shGFP was used as the control experiment. Tubulin was used as the loading control. (Right panels) Quantification of relative CIC-2 and chaperone/co-chaperone protein levels. Protein density was standardized as the ratio of the CIC-2 signal to the cognate tubulin signal. Values from the shRNA knock-down groups (hatched bars) were then normalized to those for the corresponding shGFP control (clear bars). Asterisks denote significant difference from the shGFP control (*, *t* test: $p < 0.05$; $n = 4–10$).

The results derived from the preceding shRNA knock-down experiments suggest that these molecular chaperones and co-chaperones may promote endogenous CIC-2 protein expression in mouse Leydig cells. To further verify the validity of this inference, we examined the effect of enhancing chaperone/co-chaperone expression on human CIC-2 channels heterologously expressed in HEK293T cells. As estimated from immunofluorescence analyses (data not shown), the cDNA transfection efficiency was about 70–90%. Figure 4A,B show that co-expression with Hsp90 β or Hsc70 significantly increased human CIC-2 protein level by more than 50%. Comparable protein enrichment effects were also observed when we co-expressed HOP, Aha1, or FKBP8 with human CIC-2 in HEK293T cells (Figure 4C–E).

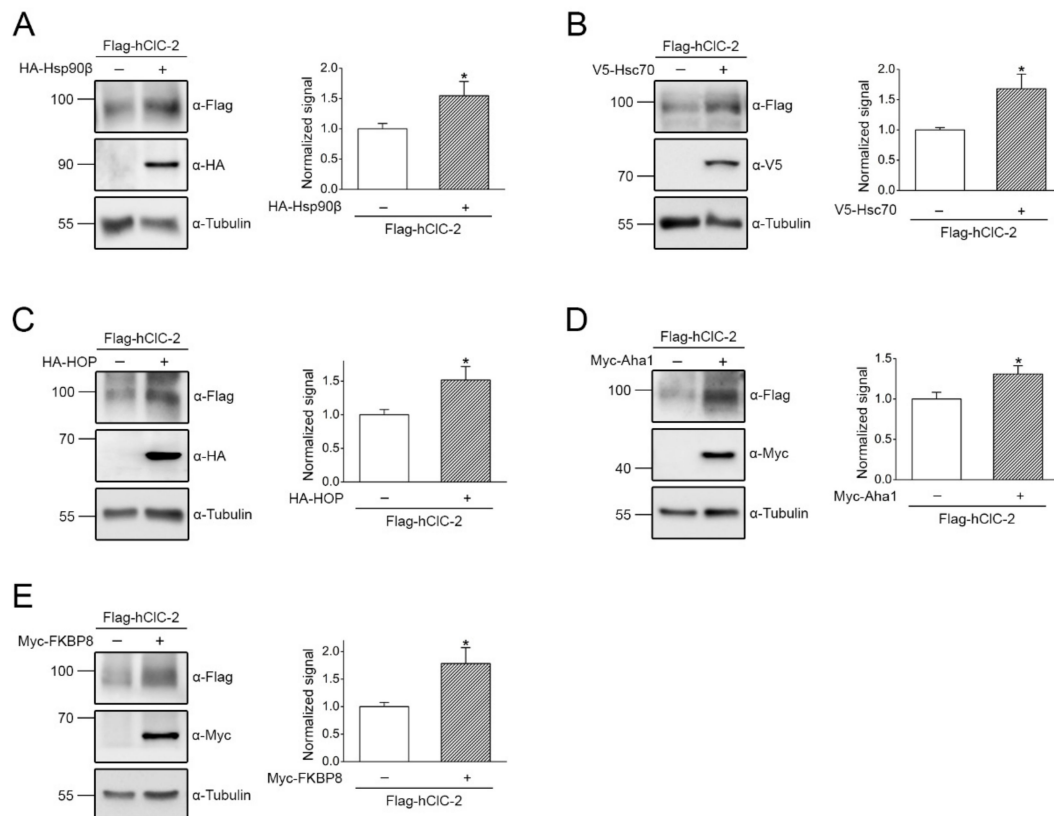


Figure 4. Co-expression with chaperone/co-chaperone increases human CIC-2 protein level in HEK293T cells. Heterologous expression of Flag-tagged human CIC-2 channels (Flag-hCIC-2) in HEK293T cells. (Left panels) Representative immunoblots showing the effect of co-expressing HA-tagged Hsp90 β (HA-Hsp90 β) (A), V5-tagged Hsc70 (V5-Hsc70) (B), HA-tagged HOP (HA-HOP) (C), Myc-tagged Aha1 (Myc-Aha1) (D), or Myc-tagged FKBP8 (Myc-FKBP8) (E) on Flag-hCIC-2 protein expression. cDNA for Flag-hCIC-2 was co-transfected with that for the indicated chaperone/co-chaperone in the molar ratio 1:3. Co-expression with the empty vector was employed as the control experiment. Tubulin was used as the loading control. (Right panels) Quantification of relative CIC-2 protein levels in the presence of various chaperones/co-chaperones. Protein density was standardized as the ratio of the CIC-2 signal to the cognate tubulin signal. Values from the chaperone/co-chaperone co-expression groups (hatched bars) were then normalized to those for the corresponding vector control (clear bars). Asterisks denote significant difference from the vector control (*, *t* test: $p < 0.05$; $n = 5–11$).

We also verified the effect of Hsp90 β co-expression on human CIC-2 heterologously expressed in CHO cells. Figure 5A illustrates that, similar to the result observed in HEK293T cells, Hsp90 β notably enhanced human CIC-2 protein level in CHO cells by about 34%. Hsp90 β co-expression also prominently increased the total protein level of the human voltage-gated potassium channel subtype 4.3 (K_V4.3) by about 68% (Figure 5B). In contrast, Hsp90 β failed to discernibly affect the protein expression of the human Ether-à-go-go-related gene (Erg) channel (Figure 5C).

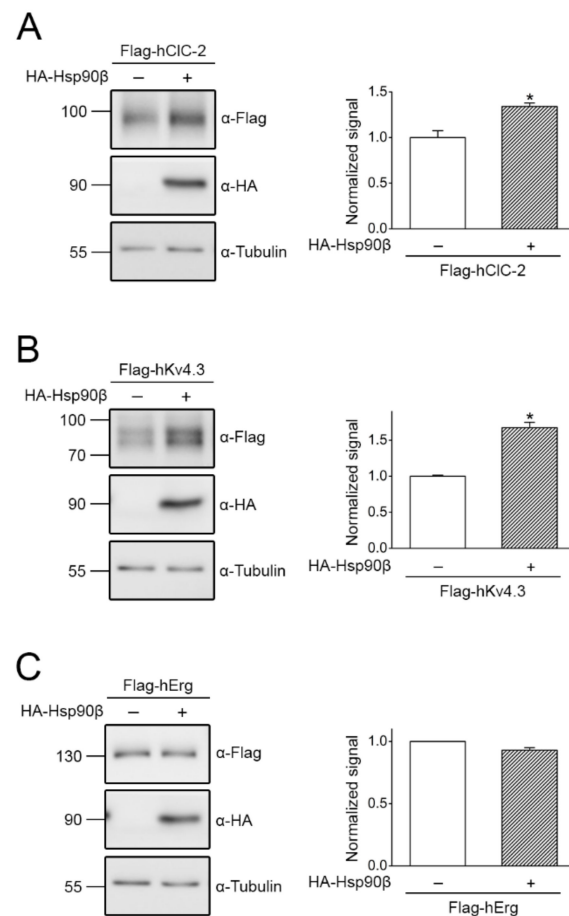


Figure 5. The effect of Hsp90 β co-expression on human CIC-2, K $_V$ 4.3, and Erg channel protein levels in CHO cells. Heterologous expression of Flag-hCIC-2 (A), Flag-tagged human K $_V$ 4.3 (Flag-hK $_V$ 4.3) (B), or Flag-tagged human Erg (Flag-hErg) (C) channels in CHO cells. (Left panels) Representative immunoblots showing the effect of HA-Hsp90 β co-expression on total protein levels. cDNA for Flag-hCIC-2/hK $_V$ 4.3/hErg was co-transfected with that for HA-Hsp90 β in the molar ratio 1:3. Co-expression with the empty vector was employed as the control experiment. Tubulin was used as the loading control. (Right panels) Quantification of relative total protein levels in response to HA-Hsp90 β co-expression. Protein density was standardized as the ratio of the CIC-2/K $_V$ 4.3/Erg signal to the cognate tubulin signal. Values from the HA-Hsp90 β co-expression groups (hatched bars) were then normalized to those for the corresponding vector control (clear bars). Asterisks denote significant difference from the vector control (*, *t* test: $p < 0.05$; $n = 3$).

2.3. Pharmacological Promotion of CIC-2 Proteostasis with Hsp90-Targeting Small Molecule

The aforementioned data indicate that CIC-2 is a client protein of Hsp90 β and its associated chaperone/co-chaperone system. Hsp90 β is known to stabilize numerous types of client proteins, including E3 ubiquitin ligases that promote degradation of misfolded proteins [41–43]. For example, Hsp90 β directly interacts with and is essential for stabilizing CUL4 [34,44], which serves as an essential component of the CUL4-DDB1-CRBN E3 ubiquitin ligase complex mediating ubiquitination and proteasomal degradation of CIC-2 channels [20]. Depending on the proteostatic role of Hsp90 β in ER quality control, pharmacological suppression of Hsp90 β activity may either enhance or reduce protein expression of its client proteins [34,45–47]. One of the well-known Hsp90-targeting small molecules is 17-allylamino-17-demethoxygeldanamycin (17-AAG), which represses Hsp90 ATPase activity by blocking ATP binding [48,49]. Interestingly, 17-AAG has been shown to effectively suppress endogenous CUL4 expression in human cells [34,46]. We therefore decided to assess the effect of 17-AAG treatment on CIC-2 protein level. Figure 6A depicts

that 24-h treatment with 1 μM 17-AAG significantly enhanced endogenous CIC-2 protein expression in mouse MA-10 Leydig cells by about 66%. In addition, 17-AAG treatment led to a more than three-fold increase in human CIC-2 protein level in human-derived HEK293T cells (Figure 6B). In contrast, 6-h treatment with 100 μM of the Hsc70/Hsp70 inhibitors 2-phenylethanesulfonamide (PES) and VER-155008 resulted in more than 70% reduction in endogenous CIC-2 protein levels in mouse MA-10 cells (Figure 6C,D). Furthermore, electrophysiological analyses revealed that 17-AAG and VER-155008 significantly promoted and suppressed, respectively, functional expression of endogenous CIC-2 channels in mouse MA-10 cells (Figure 6E). Together these observations imply that, despite of the dual role of Hsp90 β in facilitating both CIC-2 and CUL4 protein folding, suppression of Hsp90 β ATPase activity with 17-AAG results in a dominant disruption of CUL4 protein stability, thereby promoting CIC-2 protein expression.

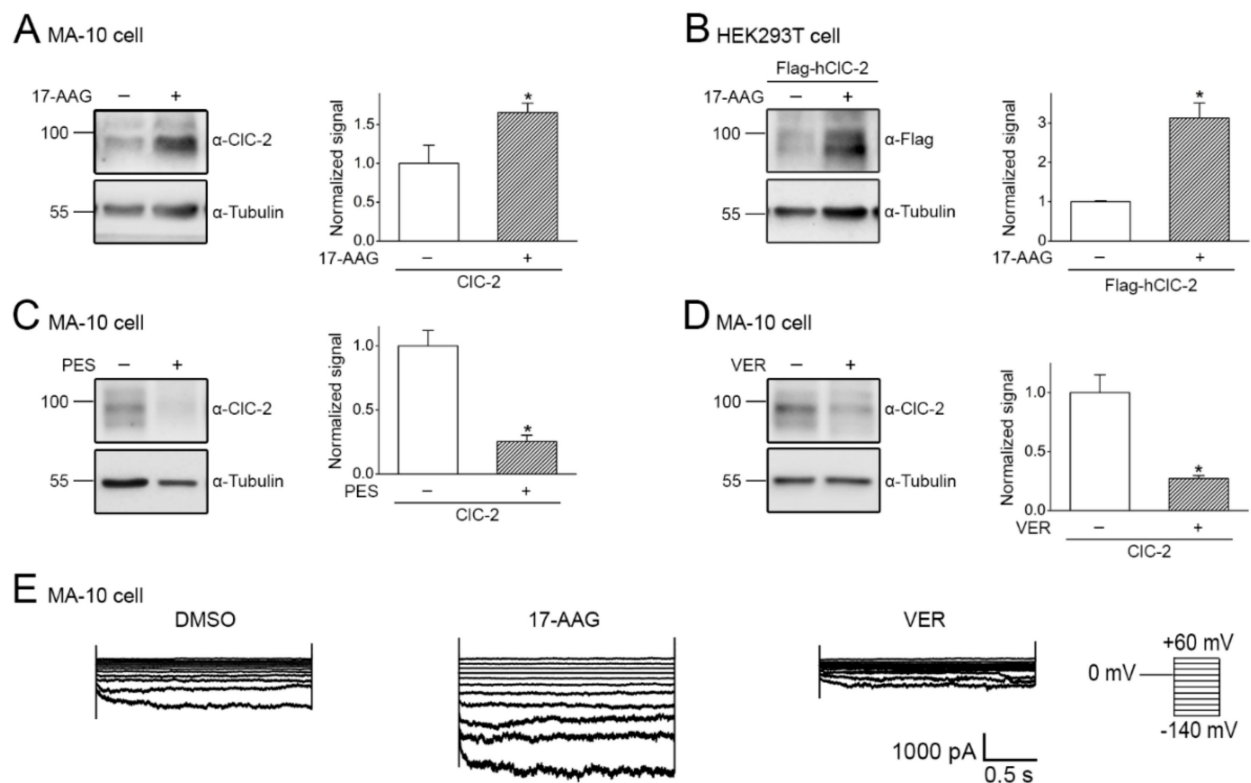


Figure 6. 17-AAG enhances total CIC-2 protein expression. (A,B) The effect of 24-h treatment of 1 μM 17-AAG (in 0.1% DMSO) on endogenous CIC-2 expression in mouse MA-10 cells (A), as well as heterologous expression of human CIC-2 in HEK293T cells (B). (Left panels) Representative immunoblots. DMSO treatment was employed as the control experiment. Tubulin was used as the loading control. (Right panels) Quantification of relative CIC-2 protein levels in response to 17-AAG treatment. Protein density was standardized as the ratio of the CIC-2 signal to the cognate tubulin signal. Values from the 17-AAG treatment group (hatched bars) were then normalized to those for the corresponding DMSO control (clear bars). Asterisks denote significant difference from the DMSO control (*, *t* test: $p < 0.05$; $n = 3-8$). (C,D) The effect of 6-h treatment with 100 μM of 2-phenylethanesulfonamide (PES) (C) or VER-155008 (VER) (D) (in 0.1% DMSO) on endogenous CIC-2 protein expression in mouse MA-10 cells. (Left panels) Representative immunoblots. (Right panels) Quantification of relative CIC-2 protein levels. Values from the PES/VER treatment group (hatched bars) were then normalized to those for the corresponding DMSO control (clear bars). Asterisks denote significant difference from the DMSO control (*, *t* test: $p < 0.05$; $n = 3$). (E) Representative endogenous CIC-2 Cl^- current traces in mouse MA-10 cells in the presence of DMSO, 17-AAG, or VER treatments. Whole-cell patch clamp recording was implemented as described in the Methods section. The voltage clamp protocol (the rightmost panel) comprises a holding potential at 0 mV, followed by 2-sec voltage pulses ranging from -140 to $+60$ mV in 20-mV increments.

So far, we have provided multiple lines of evidence showing that the Hsp90 β -associated chaperone/co-chaperone system, as well as 17-AAG treatment, promotes total CIC-2 protein expression. Since CIC-2 serves as a plasma membrane Cl⁻ channel, it is important to determine whether cell surface CIC-2 protein level is effectively enhanced as well. By performing surface biotinylation analysis, we demonstrated that 17-AAG treatment resulted in nearly four-fold increase in both total and surface human CIC-2 protein levels in HEK293T cells (Figure 7A), indicating that the majority of 17-AAG-enhanced CIC-2 protein is properly folded at the ER and therefore effectively exported to the plasma membrane. Similarly in CHO cells, both 17-AAG treatment and Hsp90 β co-expression increased total and surface human CIC-2 by about two-fold (Figure 7B,C). In comparison, 17-AAG substantially reduced total and surface human K_v4.3 protein levels in CHO cells (Figure 7B), consistent with the idea that, unlike its dual role in the ER biogenesis of CIC-2, Hsp90 β predominantly promotes K_v4.3 protein expression (Figure 7C).

Interestingly, the comparable effect of 17-AAG and Hsp90 β on total and cell surface CIC-2 protein expression (Figure 7A–C), as well as the absence of significant change in the surface-to-total protein density ratio, suggests that both 17-AAG and Hsp90 β fail to detectably modify the membrane trafficking efficiency of CIC-2. Likewise, co-expression with Hsc70, HOP, or Aha1 promoted both total and surface CIC-2 protein level to a similar extent (data not shown), indicating a lack of measurable change in membrane trafficking efficiency. Nevertheless, FKBP8 co-expression resulted in about two-fold and six-fold increases in total and surface CIC-2, respectively (Figure 7D). This significant enhancement of the surface-to-total CIC-2 protein density ratio implies that, in addition to promoting protein folding at the ER, FKBP8 may also facilitate the membrane trafficking process of CIC-2 channels.

2.4. Correction of Disease-Related Defective CIC-2 Expression by 17-AAG

Two mutations located at the membrane-passing helix O of the human CIC-2 channel, A500V and G503R, have been linked to leukodystrophy [11,13,14]. Figure 8A illustrates that, compared to their WT counterpart, the total protein level of the two mutants was significantly decreased, consistent with the presence of anomalous proteostasis in disease-causing CIC-2 mutant channels. Surface biotinylation analyses further indicated that the CIC-2 A500V and G503R mutants were associated with substantially reduced cell surface expression, as well as notable defects in membrane trafficking efficiency (Figure 8B). Importantly, in response to 17-AAG treatment, the total protein level of the two leukodystrophy-causing CIC-2 mutants was enhanced by about 2-fold (Figure 9A,B). Moreover, 17-AAG substantially increased cell surface expression of the mutants by 75% or more (Figure 9C,D), indicating that a notable fraction of 17-AAG-rescued CIC-2 A500V and G503R proteins can be successfully transported from the ER to the plasma membrane.

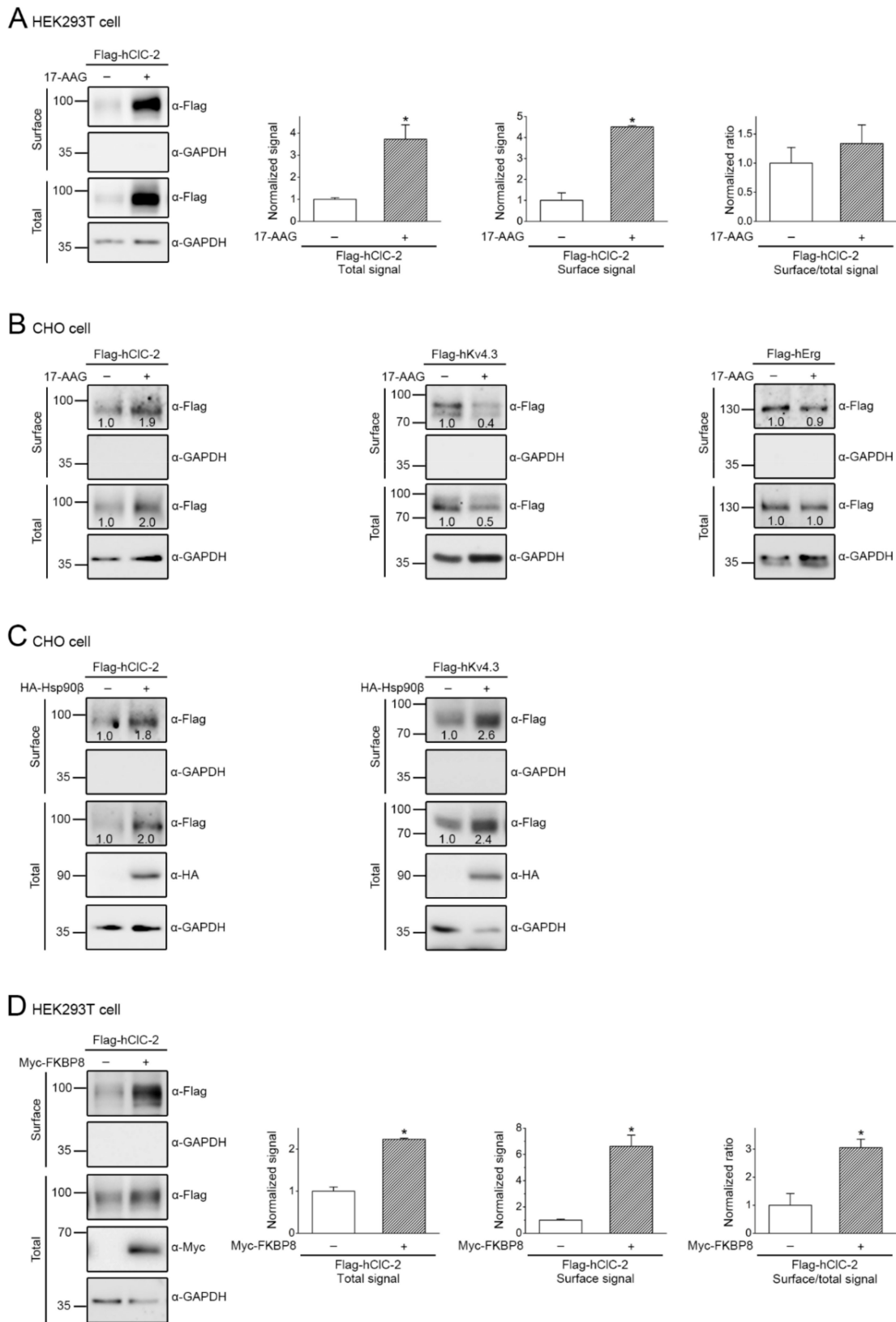


Figure 7. 17-AAG, Hsp90β, and FKBP8 promote cell surface expression of human CIC-2 channels. (A) The effect of 24-h treatment of 1 μM 17-AAG (in 0.1% DMSO) on surface biotinylation experiments in HEK293T cells over-expressing human

CIC-2. (Left panel) Representative immunoblots. Cell lysates from biotinylated intact cells were either directly employed for immunoblotting analyses (total) or subject to streptavidin pull-down prior to immunoblotting analyses (surface). GAPDH was used as the loading control. (Right panels) Quantification of surface protein level and surface expression efficiency (surface/total). The surface protein density was standardized as the ratio of surface signal to cognate total GAPDH signal, followed by normalization to that of the control (clear bars). The total protein density was standardized as the ratio of input signal to GAPDH signal. Surface expression efficiency was calculated as surface protein density divided by the corresponding total protein density, followed by normalization with respect to the surface-to-total ratio of the DMSO control (clear bars). Asterisks denote significant difference from the DMSO control (*, *t* test: $p < 0.05$; $n = 4$). (B,C) Representative immunoblots showing the effect of 17-AAG treatment (B) or Hsp90 β co-expression (C) on surface biotinylation experiments in CHO cells over-expressing the indicated human ion channels. The numbers on the immunoblots denote the relative channel protein levels with respect to the control condition. (D) The effect of FKBP8 co-expression on surface biotinylation experiments in HEK293T cells over-expressing human CIC-2. (Left panel) Representative immunoblots. (Right panels) Quantification of surface protein level and surface expression efficiency. Asterisks denote significant difference from the vector control (*, *t* test: $p < 0.05$; $n = 4$).

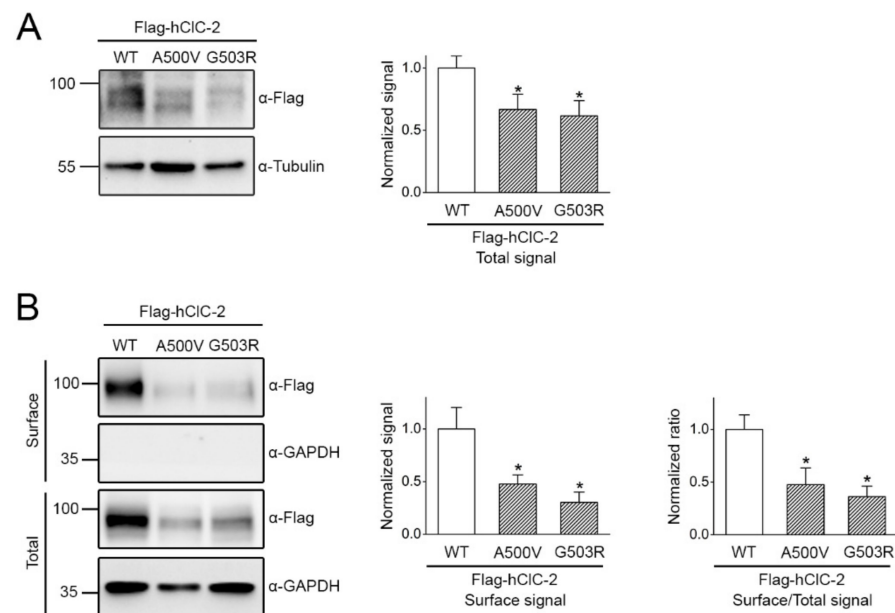


Figure 8. Leukodystrophy-causing mutant CIC-2 channels display reduced total and surface protein expressions, as well as impaired membrane trafficking efficiency. Human CIC-2 WT and leukodystrophy-associated A500V and G503R mutants were over-expressed in HEK293T cells. (A) (Left panel) Representative immunoblot comparing total protein level. (Right panel) Quantification of relative CIC-2 total protein level. Protein density was standardized as the ratio of the CIC-2 signal to the cognate tubulin signal. Values from the mutant groups (hatched bars) were then normalized to those for the corresponding WT control (clear bars). Asterisks denote significant difference from the WT (*, *t* test: $p < 0.05$; $n = 5$). (B) (Left panel) Representative immunoblot comparing surface protein level. (Right panels) Quantification of relative CIC-2 surface protein level and surface expression efficiency (surface/total). The surface protein density was standardized as the ratio of surface signal to cognate total GAPDH signal, followed by normalization to that of the WT control (clear bars). The surface expression efficiency was calculated as surface protein density divided by the corresponding total protein density, followed by normalization with respect to the surface-to-total ratio of the corresponding WT control (clear bars). Asterisks denote significant difference from the WT (*, *t* test: $p < 0.05$; $n = 5$).

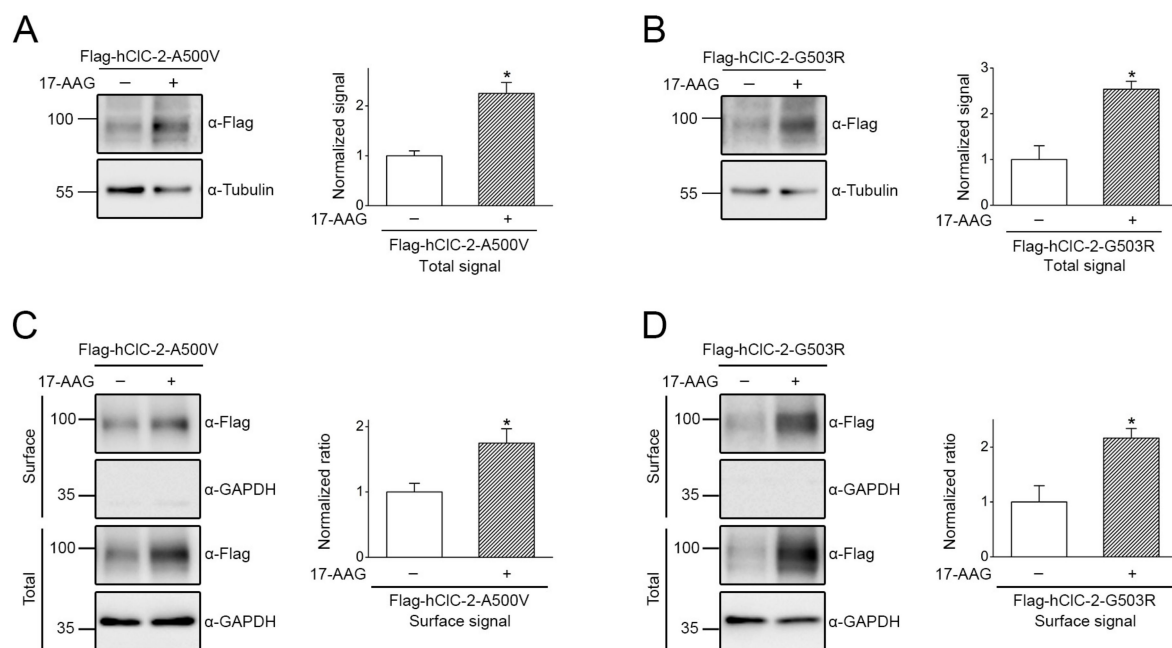


Figure 9. 17-AAG ameliorates defective protein expression of human CIC-2 mutants. The effect of 17-AAG treatment on total (A,B) and surface (C,D) protein levels of the human CIC-2 A500V and G503R mutants. Heterologous expression of leukodystrophy-associated mutant human CIC-2 proteins in HEK293T cells was subject to 24-h treatment of 1 μ M 17-AAG (in 0.1% DMSO). DMSO treatment was employed as the control experiment. (Left panels) Representative immunoblot. (Right panels) Quantification of relative CIC-2 protein level. Protein density was standardized as the ratio of the CIC-2 signal to the cognate tubulin signal. Values from the 17-AAG treatment group (hatched bars) were then normalized to those for the corresponding DMSO control (clear bars). Asterisks denote significant difference from the DMSO control (*, *t* test: $p < 0.05$; $n = 4-8$).

3. Discussion

In this study, we aim to ascertain the molecular nature of the ER quality control system for CIC-2 Cl⁻ channels. As summarized in the schematic model illustrated in Figure 10, we propose that CIC-2 protein biogenesis at the ER is promoted by the Hsp90 β -Hsc70 chaperone system associated with the co-chaperones HOP, Aha1, and FKBP8. In contrast, leukodystrophy-causing mutations tend to disrupt CIC-2 protein folding at the ER, leading to enhanced CIC-2 polyubiquitination by the CUL4-DDB1-CRBN E3 ubiquitin ligase complex and the ensuing proteasomal degradation [20].

Both our shRNA knock-down and chaperone over-expression data (Figures 3–5) support the idea that the primary role of Hsp90 β in ER quality control of CIC-2 involves a protein stabilization effect. However, Hsp90 β also contributes to protein stabilization of CUL4 [34,44], the essential scaffold protein of the CUL4-DDB1-CRBN E3 ligase promoting ER-associated degradation of CIC-2 [20]. In other words, Hsp90 β may play a dual role in regulating CIC-2 proteostasis at the ER: (i) directly promoting CIC-2 protein expression, but (ii) indirectly enhancing CIC-2 degradation via stabilizing CUL4. Nonetheless, pharmacological interruption of Hsp90 β function with 17-AAG results in significant up-regulation of total and surface CIC-2 protein levels (Figures 6 and 7), suggesting that 17-AAG may exert a dominant inhibition of the molecular chaperone's effect on CUL4 protein stability. 17-AAG has been previously demonstrated to raise the protein level of another voltage-gated Cl⁻ channel, CIC-1 [34]. Interestingly, loss-of-function mutations in the human *CLCN1* gene encoding CIC-1 are associated with the skeletal muscle disease myotonia congenita and manifest aberrant proteostasis and gating of the Cl⁻ channel [5,50]. Both CIC-1 and CIC-2 belong to the CLC channel/transporter superfamily that includes three additional types of Cl⁻ channels [5,51,52]. Moreover, similar to the proteostatic mechanism of CIC-2, the CUL4-DDB1-CRBN E3 ligase complex promotes ER-associated degradation of the CIC-1 channel [53], and the Hsp90 β -Hsc70 chaperone/co-chaperone system works in concert

to promote CIC-1 protein folding at the ER [34]. It remains to be determined whether suppressing the ATPase function of Hsp90 β with 17-AAG may facilitate ER proteostasis for the other members of the CLC channel/transporter superfamily as well.

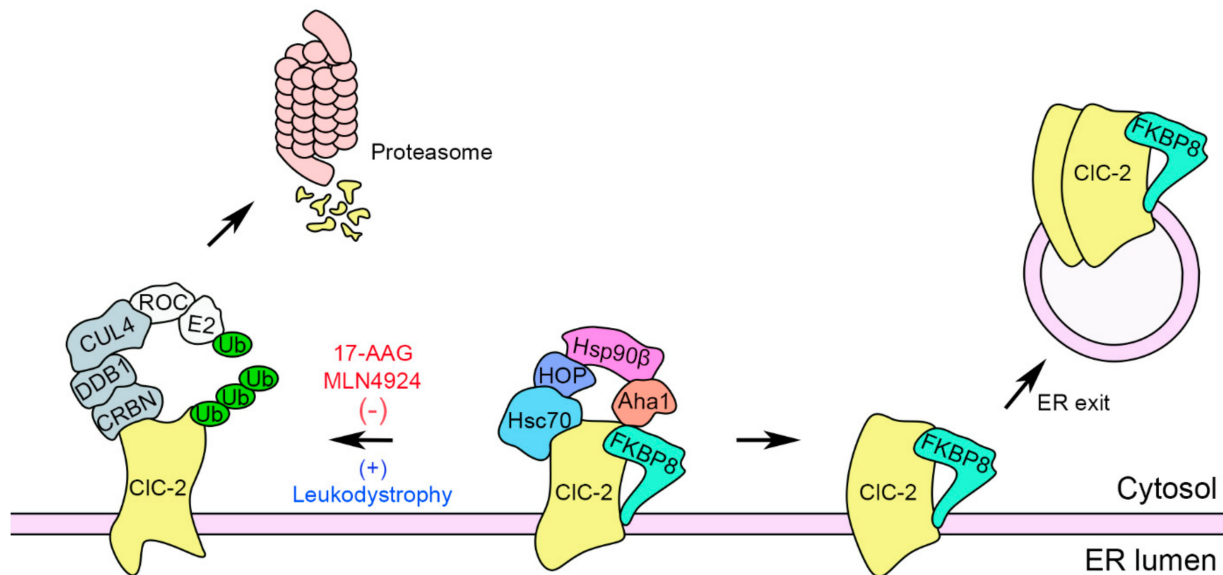


Figure 10. Schematic model of the ER quality control system for CIC-2 channels. In this schematic diagram of CIC-2 protein biogenesis at the ER, protein folding is primarily promoted by the constitutively expressed chaperones Hsp90 β and Hsc70, as well as the co-chaperones HOP, Aha1, and FKBP8. FKBP8 may additionally contribute to a late stage of the CIC-2 protein folding process essential for subunit assembly, ER exit, and thereafter membrane trafficking. On the other hand, ER-associated degradation of CIC-2 is principally mediated by the scaffold protein CUL4 that forms a protein complex with the adaptor protein DDB1 and the substrate receptor protein CRBN. CUL4 also interacts with the RING-finger protein ROC, which recruits the E2 ubiquitin conjugating enzyme (E2) that transfers ubiquitin (Ub) for covalent linkage to a substrate protein. The CUL4-DDB1-CRBN E3 ubiquitin ligase complex catalyzes the ubiquitination of misfolded CIC-2 proteins. Ubiquitinated CIC-2 is subsequently targeted for proteasomal degradation. Leukodystrophy-causing mutations may instigate substantial protein misfolding that leads to increased CIC-2 protein degradation. In contrast, the Hsp90 inhibitor 17-AAG, as well as the cullin E3 ligase inhibitor MLN4924, significantly attenuates protein ubiquitination of CIC-2 channels, resulting in enhanced total and surface CIC-2 protein levels.

In normal and stressed conditions alike, the constitutively expressed Hsc70 chaperone is essential for ER proteostasis, maintaining both protein folding and degradation [54,55]. For example, Hsc70 has been implicated in hereditary ion channel diseases such as cystic fibrosis and long QT syndrome, wherein Hsc70 partially contributes to protein folding at the ER but plays a critical role in promoting ER-associated degradation of disease-causing mutant ion channels [55,56]. Of note, Hsc70 and Hsp90 are also known to critically promote protein degradation and folding/trafficking, respectively, of steroid receptors [57–59]. In comparison, the primary role of Hsc70 in ER quality control of WT and disease-related CIC-1/CIC-2 channels is facilitation of protein folding (Figures 3 and 4) [34]. One potential explanation for this apparent contrast in the functional character of Hsc70 in protein biogenesis may concern the molecular nature of the E3 ubiquitin ligase coupled with the molecular chaperone system: the former example involves carboxyl terminus Hsc70-interacting protein (CHIP), and the latter Hsp90 β -interacting CUL4-DDB1-CRBN complex. Further investigation is required to determine whether and how E3 ubiquitin ligase is coupled with the proteostatic role of Hsc70 in protein folding and degradation.

As highlighted in the biotinylation data in Figure 7D, as well as the schematic diagram in Figure 10, FKBP8 is unique among the three identified CIC-2-interacting co-chaperones in that it promotes protein folding at the ER, as well as assisting membrane trafficking of CIC-2 channels. This observation implies that FKBP8 may additionally contribute to a late-stage ER protein folding process essential for ER exit and subsequent membrane trafficking. Im-

portantly, FKBP8 also effectively facilitates membrane trafficking of the CIC-1 channel [34]. Moreover, FKBP8 may directly stabilize protein conformation of CIC-1 channels localized at the plasma membrane [60]. In contrast, despite its well established role in ER biogenesis, FKBP8 does not appear to contribute to trafficking and membrane stabilization of WT and mutant Cl⁻ channels implicated in cystic fibrosis [61]. It remains an open question whether the membrane trafficking effect of FKBP8 is specific for CIC-1 and CIC-2 channels only, or may be applicable to the other members of the CLC channel/transporter superfamily.

We report here that the Hsp90 inhibitor 17-AAG substantially increases total and cell surface protein levels of disease-associated loss-of-function CIC-2 mutant channels (Figure 9). Notably, 17-AAG has been extensively tested in a wide variety of different clinical trials as a tumor suppression drug [48,49,62], as well as a chemical chaperone for correcting anomalous proteostasis associated with neurodegenerative diseases [22,63,64]. In addition, we previously demonstrated that the CUL4 inhibitor MLN4924, an emerging anti-cancer drug [65–69], also effectively promotes protein expression of leukodystrophy-related CIC-2 mutant channels [20]. Taken together, as emphasized in the schematic model illustrated in Figure 10, our findings highlight the therapeutic potential of 17-AAG and MLN4924 as clinically applicable small molecules for correcting impaired ER proteostasis of leukodystrophy-causing, loss-of-function CIC-2 mutant proteins.

4. Materials and Methods

4.1. cDNA Constructs

Human CIC-2 cDNA (NM_004366) was subcloned into the pcDNA3-Flag vector (Invitrogen, Carlsbad, CA, USA) to generate the N-terminal Flag-tagged human CIC-2 (Flag-hCIC-2) construct. Leukodystrophy-causing CIC-2 mutations (A500V and G503R) were generated by site-directed mutagenesis, followed by verification with DNA sequencing. Other cDNA constructs employed in this study include pcDNA3.1-Myc mouse Aha1, pcDNA3.1-Myc mouse FKBP8, pFlag-CMV2 human Erg, pcDNA3-HA rat HOP, pcDNA5-V5 human Hsc70 (Addgene 19514, Watertown, MA, USA), pcDNA3-HA human Hsp90 β (Addgene 22847, Watertown, MA, USA), and pcDNA3-Flag human Kv4.3.

4.2. Preparation of Animal Samples for Co-Immunoprecipitation

C57BL/6 mice were handled in accordance with the National Institute of Health Guide for the Care and Use of Laboratory Animals (NIH Publications No. 80-23, revised 1996, Bethesda, MD, USA). All procedures involving animals were performed in conformity with the animal protocol approved by the Institutional Animal Care and Use Committee (IACUC), College of Medicine, National Taiwan University.

Testes dissected from mice (about 6-weeks-old; weighing about 19 g) were homogenized in ice-cold T-PER tissue extraction reagent (Thermo Scientific, Waltham, MA, USA; 1 testis per 400 μ L) containing protease inhibitor cocktail. Lysates were cleared by microcentrifugation at 13,360 \times g for 15 min. Solubilized lysates were pre-cleared with protein G sepharose beads (GE Healthcare Biosciences, Piscataway Township, NJ, USA) for 2 h at 4 °C, and then incubated for 16 h at 4 °C with protein G sepharose beads pre-coated with rabbit IgG or rabbit anti-CIC-2 antibody. Beads were gently spun down and washed twice in a wash buffer [(in mM) 100 NaCl, 4 KCl, 2.5 EDTA, 20 NaHCO₃, 20 Tris-HCl, pH 7.5] supplemented with 0.1% Triton X-100, and then twice with the wash buffer. The immune complexes were eluted from the beads by heating at 70 °C for 5 min in the Laemmli sample buffer.

4.3. Cell Culture and DNA Transfection

Mouse MA-10 Leydig cells and Chinese hamster ovary (CHO) cells were maintained in Dulbecco's modified Eagle's medium (DMEM)/F12 supplemented with 10% fetal bovine serum and 20 mM HEPES. HEK293T cells were grown in DMEM supplemented with 2 mM glutamine, 10% fetal bovine serum (Thermo Scientific, Waltham, MA, USA), 100 units/mL penicillin, and 50 μ g/mL streptomycin, and were maintained at 37 °C in a humidified

incubator with 5% CO₂. Transient transfection in HEK293T and CHO cells was performed by using the Lipofectamine 2000 reagent (Invitrogen, Carlsbad, CA, USA). Cells were plated onto 12-well plates 24 hrs before transfection. Various expression constructs were incubated with the transfection reagent for 20 min at room temperature, and DNA-lipofectamine diluted in Opti-MEM (Invitrogen, Carlsbad, CA, USA) was added to culture wells. After 6-h incubation at 37 °C, the medium was changed and the culture cells were maintained in the 37 °C incubator for 48 hrs. Where indicated, 17-AAG, 2-phenylethynylsulfonamide (PES; also known as pifithrin- μ), and VER-155008 (Sigma, St. Louis, MO, USA), dissolved in 0.1% dimethyl sulfoxide (DMSO), was applied to the culture medium.

4.4. RNA Interference

Lentivirus-based shRNA constructs (subcloned into the pLKO vector) targeting specific Aha1 (5'-CCCTGAGAAACATATTGTGAT-3'), FKBP8 (5'-AGTGGACATGACGTTCCGAGGA-3'), CIC-2 (5'-CCTAGCTCCGAGACATCTATC-3'), HOP (5'-CGACCTTCATCAAGGGTTATA-3'), Hsc70 (5'-CGTCTGATTGGACGCAGATTT-3'), or Hsp90 β (5'-CTTGTGTTGAA GGCAGTAAAC-3') sequences, as well as the control shRNA for LacZ (5'-TGTTTCGCATTATCCGAACCAT-3') and GFP (5'-GACCACCCTGACCTACGGCGT-3'), were purchased from National RNAi Core Facility, Taiwan. Recombinant lentivirus was generated by co-transfecting HEK293T cells with the packaging plasmid pCMV- Δ R8.91, the envelope plasmid pMD.G, and shRNA expressing constructs via the jetPRIME transfection reagent (Polyplus-transfection, Illkirch, France). Then, 48 h after transfection, the medium was collected on a daily basis (stored at -80 °C; followed by application of new medium to HEK293T cells) for three consecutive days. The collected media containing lentiviral particles were centrifuged at 3000 \times g for 5 min, and supernatants were harvested and filtered (0.22 μ m). MA-10 cells were maintained in the freshly collected viral supernatants in the presence of 8 μ g/mL polybrene (Sigma, St. Louis, MO, USA) for at least 48 h, followed by incubation with a selection medium containing puromycin (5 μ g/mL) for at least 48 h.

4.5. Immunoblotting

MA-10, HEK293T, and CHO cells were washed twice with ice-cold Dulbecco's phosphate buffered saline (D-PBS) [(in mM) 137 NaCl, 2.7 KCl, 4.3 Na₂HPO₄·2H₂O, 1.4 KH₂PO₄, pH 7.3] supplemented with 2 mM EDTA, and resuspended in a lysis buffer [(in mM) 150 NaCl, 5 EDTA, 50 Tris-HCl pH 7.6, 1% Triton X-100] containing a complete protease inhibitor cocktail (Roche, Basel, Switzerland). After adding the Laemmli sample buffer to the lysates, samples were sonicated on ice (three times for five seconds each) and heated at 70 °C for 5 min. Samples were then separated by 7.5–10% SDS-PAGE, electrophoretically transferred to nitrocellulose membranes, and detected using rabbit anti-Aha1 (1:2500; Thermo Scientific, Waltham, MA, USA), rabbit-anti-CIC-2 (1:1000; Alomone, Jerusalem, Israel), rabbit anti-Flag (1:5000; Sigma, St. Louis, MO, USA), rabbit anti-FKBP8 (1:4000; EnoGene, New York, NY, USA), rabbit anti-glyceraldehyde-3-phosphate dehydrogenase (GAPDH) (1:5000; GeneTex, Irvine, CA, USA), rat anti-HA (1:5000; Roche, Basel, Switzerland), rabbit anti-HOP (1:10000; Abcam, Cambridge, UK), rabbit anti-Hsc70 (1:750; Abcam, Cambridge, UK), rabbit anti-Hsp90 β (1:500; Abcam, Cambridge, UK), mouse anti-Myc (clone 9E10), or rabbit anti- α -tubulin (1:5000; GeneTex, Irvine, CA, USA) antibodies. Blots were then exposed to horseradish peroxidase-conjugated anti-mouse/rabbit IgG (1:5000; Jackson ImmunoResearch, West Grove, PA, USA) or goat anti-rat IgG (1:5000; Santa Cruz, Dallas, TX, USA), and revealed by an enhanced chemiluminescence detection system (Thermo Scientific, Waltham, MA, USA). Where necessary, horseradish peroxidase-conjugated Easy-Blot anti-rabbit IgG (GeneTex, Irvine, CA, USA) was employed as the secondary antibody to obscure the signal associated with rabbit heavy or light immunoglobulin chains. Acquisition of chemiluminescent signals from immunoblots was achieved by using the UVP AutoChemi image system (Ultra-Violet Products, Upland, CA, USA). Results shown are representative of at least three independent experiments.

For quantitative analyses, data were collected from at least three independent experiments performed in duplicates or triplicates. Densitometric scans of immunoblots were quantified by using ImageJ (National Institute of Health, Bethesda, MD, USA). For a given immunoblot containing multiple lanes of protein signals associated with the same experimental condition addressing a specific issue, protein density was first standardized as the ratio of the densitometric signal of the protein of interest to that of the cognate loading control. Standardized protein density values of all the control groups were then used for calculating the mean control protein density. Standardized protein density values of individual treatment or control groups were subsequently normalized with respect to the mean control protein density. For a given experimental condition with multiple repeats, normalized protein density values from multiple immunoblots were pooled together for statistical analyses.

4.6. Immunofluorescence

MA-10 cells grown on coverslips were rinsed in ice-cold phosphate buffered saline (PBS) and fixed with 4% paraformaldehyde at room temperature for 20 min, or with cold methanol at $-20\text{ }^{\circ}\text{C}$ for 10 min. After being washed with cold PBS, fixed cells were permeabilized and blocked with a blocking buffer (5% normal goat serum in 20 mM phosphate buffer, pH 7.4, 0.1% (*v/v*) Triton X-100, and 0.45 M NaCl) for 60 min at $4\text{ }^{\circ}\text{C}$. Cells were then immunolabeled overnight at $4\text{ }^{\circ}\text{C}$ with 1:200 dilution (in the blocking buffer) of rabbit anti-Aha1, mouse anti-CIC-2 (Santa Cruz, Dallas, TX, USA), rabbit anti-FKBP8, rabbit anti-HOP, rabbit anti-Hsc70, or rabbit anti-Hsp90 β antibodies. Alexa Fluor 488-conjugated anti-rabbit IgG and Alexa Fluor 568-conjugated anti-mouse IgG (1:200; Molecular Probes, Eugene, OR, USA) were used as secondary antibodies. Nuclei were stained with DAPI. After final wash, coverslips were mounted in a mounting medium (4% n-propylgallate, 90% glycerol, 0.1 M carbonate buffer, pH 9.2). Fluorescence images were viewed and acquired with a confocal microscope (TCS SP8, Leica, Wetzlar, Germany).

4.7. Electrophysiology

Conventional whole-cell patch clamp techniques were employed to record endogenous CIC-2 Cl⁻ currents in MA-10 cells. Cells were kept in the bath solution comprising (in mM): 140 NaCl, 4 CsCl, 2 MgCl₂, 2 CaCl₂, 10 HEPES, pH 7.4. Glass pipette electrodes with a resistance of 2–3 M Ω were filled with the intracellular solution containing (in mM): 120 CsCl, 10 EGTA, 10 HEPES, pH 7.4. Data were acquired and digitized with Axopatch 200A and Digidata 1322A, respectively, via pCLAMP 10 (Molecular Devices, San Jose, CA, USA). Cell capacitances were measured using a built-in function of pCLAMP 10 and were compensated electronically with Axopatch 200A. The holding potential was set at 0 mV. Data were sampled at 10 kHz and filtered at 1 kHz. All recordings were performed at room temperature (20–22 $^{\circ}\text{C}$).

4.8. Cell Surface Biotinylation

HEK293T and CHO cells were rinsed with ice-cold D-PBS supplemented with 0.5 mM CaCl₂, 2 mM MgCl₂, incubated in 1 mg/mL sulfo-NHS-LC-biotin (Thermo Scientific, Waltham, MA, USA) in D-PBS at $4\text{ }^{\circ}\text{C}$ for 1 h with gentle rocking on an orbital shaker, and subject to a quenching procedure by removing the biotin reagents and rinsing 3 times with 100 mM glycine in PBS, followed by once in Tris buffered saline [(in mM) 20 Tris-HCl, 150 NaCl, pH 7.4]. Cells were solubilized in ice-cold lysis buffer [(in mM) 150 NaCl, 50 Tris-HCl, 1% Triton X-100, 5 EDTA, 1 PMSE, pH 7.6] supplemented with protease inhibitor cocktail. Insolubilized materials were removed by centrifugation at $4\text{ }^{\circ}\text{C}$. Solubilized cell lysates were incubated overnight at $4\text{ }^{\circ}\text{C}$ with streptavidin-agarose beads (Thermo Scientific, Waltham, MA, USA). Beads were washed once in the lysis buffer, followed by twice in a high-salt buffer [(in mM) 500 NaCl, 5 EDTA, 50 Tris-HCl, pH 7.6, 0.1% Triton X-100] and once in a low-salt buffer [(in mM) 2 EDTA, 10 Tris-HCl, pH 7.6, 0.1% Triton

X-100]. Biotin-streptavidin complexes were eluted from the beads by heating at 70 °C for 5 min in the Laemmli sample buffer.

Cell lysates from biotinylated intact cells were subject to either direct immunoblotting analyses (regarded as total protein level; *total*) or streptavidin pull-down prior to immunoblotting analyses (regarded as surface protein level; *surface*). During sample loading for SDS-PAGE, the amount of lysates loaded in the *total* lane represents about 8% of that loaded in the *surface* lane. For quantitative analyses of *total* and *surface* signals, protein density was standardized as the ratio to the cognate loading control in the *total* lane. Surface expression efficiency (*surface/total*) was calculated as surface protein density divided by the corresponding standardized total protein density, followed by normalization with respect to the surface-to-total ratio of the control.

4.9. Statistical Analyses

All values were presented as mean \pm SEM. Based on the assumption of normality and homogeneity of variance, the significance of the difference between two means was tested using the Student's *t* test, whereas means from multiple groups were compared using the one-way ANOVA analysis, followed by post hoc analysis with the Bonferroni *t* test. All statistical analyses were performed with Origin 7.0 (Microcal Software, Northampton, MA, USA).

Author Contributions: Conceptualization, M.-C.H., T.-Y.C., C.-J.J. and C.-Y.T.; Methodology, S.-J.F., M.-C.H. and A.-T.C.; Formal Analysis, S.-J.F., C.-T.H. and A.-T.C.; Data Curation, C.-J.J. and C.-Y.T.; Writing—Original Draft Preparation, C.-J.J. and C.-Y.T.; Writing—Review & Editing, C.-J.J. and C.-Y.T.; Visualization, S.-J.F. and C.-T.H.; Funding Acquisition, M.-C.H., T.-Y.C., C.-J.J. and C.-Y.T. All authors have read and agreed to the published version of the manuscript.

Funding: This work was supported by research grants from Ministry of Science and Technology, Taiwan to M.-C.H. (109-2320-B-002-015-MY3), C.-J.J. (108-2320-B-010-039-MY3), and C.-Y.T. (108-2320-B-002-033-MY3), from Ministry of Education, Taiwan, for The Brain Research Center of National Yang Ming Chiao Tung University on the Higher Education Sprout Project (109BRC-B404) to C.-J.J. and from National Institutes of Health, USA (R01GM065447) to T.-Y.C.

Institutional Review Board Statement: All procedures involving animals were performed in conformity with the animal protocol approved by the Institutional Animal Care and Use Committee (IACUC), College of Medicine, National Taiwan University (protocol code 2018358; date of approval: 27 February 2019).

Informed Consent Statement: Not applicable.

Data Availability Statement: The data that support the findings of this study are available from the corresponding authors, upon reasonable request.

Acknowledgments: We thank Chih-Yu Tang and Rong-Whei Chao for technical assistance.

Conflicts of Interest: The authors declare no competing financial interests.

Abbreviations

17-AAG	17-allylamino-17-demethoxygeldanamycin
Aha1	activator of Hsp90 ATPase homolog 1
CHIP	carboxyl terminus Hsc70-interacting protein
Cl ⁻	chloride
CHO	Chinese hamster ovary
CRBN	cereblon
CUL	cullin
DDB	damage-specific DNA binding protein
D-PBS	Dulbecco's phosphate buffered saline
DMEM	Dulbecco's modified Eagle's medium
DMSO	dimethyl sulfoxide
DTT	dithiothreitol

ER	endoplasmic reticulum
Erg	Ether-à-go-go-related gene
FKBP8	FK506-binding protein 8
GAPDH	glyceraldehyde-3-phosphate dehydrogenase
HEK	human embryonic kidney
HOP	Hsp70/Hsp90 organizing protein
Hsc70	heat shock cognate protein 70
Hsp90 β	heat shock protein 90 β
IP	immunoprecipitation
K _V 4.3	voltage-gated potassium channel subtype 4.3
PBS	Phosphate buffered saline
PES	2-phenylethanesulfonamide
PMSF	phenylmethylsulfonyl fluoride
WT	wild-type

References

- Cid, L.P.; Montrose-Rafizadeh, C.; Smith, D.I.; Guggino, W.B.; Cutting, G.R. Cloning of a putative human voltage-gated chloride channel (CIC-2) cDNA widely expressed in human tissues. *Hum. Mol. Genet.* **1995**, *4*, 407–413. [[CrossRef](#)]
- Thiemann, A.; Grunder, S.; Pusch, M.; Jentsch, T.J. A chloride channel widely expressed in epithelial and non-epithelial cells. *Nature* **1992**, *356*, 57–60. [[CrossRef](#)]
- Sik, A.; Smith, R.L.; Freund, T.F. Distribution of chloride channel-2-immunoreactive neuronal and astrocytic processes in the hippocampus. *Neuroscience* **2000**, *101*, 51–65. [[CrossRef](#)]
- Gyomory, K.; Yeager, H.; Ackerley, C.; Garami, E.; Bear, C.E. Expression of the chloride channel CIC-2 in the murine small intestine epithelium. *Am. J. Physiol. Cell Physiol.* **2000**, *279*, C1787–C1794. [[CrossRef](#)] [[PubMed](#)]
- Jentsch, T.J.; Pusch, M. CLC Chloride Channels and Transporters: Structure, Function, Physiology, and Disease. *Physiol. Rev.* **2018**, *98*, 1493–1590. [[CrossRef](#)]
- Grunder, S.; Thiemann, A.; Pusch, M.; Jentsch, T.J. Regions involved in the opening of CIC-2 chloride channel by voltage and cell volume. *Nature* **1992**, *360*, 759–762. [[CrossRef](#)] [[PubMed](#)]
- Jordt, S.E.; Jentsch, T.J. Molecular dissection of gating in the CIC-2 chloride channel. *EMBO J.* **1997**, *16*, 1582–1592. [[CrossRef](#)] [[PubMed](#)]
- Nehrke, K.; Arreola, J.; Nguyen, H.-V.; Pilato, J.; Richardson, L.; Okunade, G.; Baggs, R.; Shull, G.E.; Melvin, J.E. Loss of hyperpolarization-activated Cl⁻ current in salivary acinar cells from Clcn2 knockout mice. *J. Biol. Chem.* **2002**, *277*, 23604–23611. [[CrossRef](#)]
- Bösl, M.R.; Stein, V.; Hübner, C.; Zdebik, A.A.; Jordt, S.-E.; Mukhopadhyay, A.K.; Davidoff, M.S.; Holstein, A.-F.; Jentsch, T.J. Male germ cells and photoreceptors, both dependent on close cell-cell interactions, degenerate upon CIC-2 Cl⁻ channel disruption. *EMBO J.* **2001**, *20*, 1289–1299. [[CrossRef](#)] [[PubMed](#)]
- Blanz, J.; Schweizer, M.; Auberson, M.; Maier, H.; Muenscher, A.; Hubner, C.A.; Jentsch, T.J. Leukoencephalopathy upon disruption of the chloride channel CIC-2. *J. Neurosci.* **2007**, *27*, 6581–6589. [[CrossRef](#)] [[PubMed](#)]
- Depienne, C.; Bugiani, M.; Dupuits, C.; Galanaud, D.; Touitou, V.; Postma, N.; van Berkel, C.; Polder, E.; Darios, F.; et al. Brain white matter oedema due to CIC-2 chloride channel deficiency: An observational analytical study. *Lancet Neurol.* **2013**, *12*, 659–668. [[CrossRef](#)]
- Guo, Z.; Lu, T.; Peng, L.; Cheng, H.; Peng, F.; Li, J.; Lu, Z.; Chen, S.; Qiu, W. CLCN2-related leukoencephalopathy: A case report and review of the literature. *BMC Neurol.* **2019**, *19*, 156.
- Gaitán-Peñas, H.; Apaja, P.M.; Arnedo, T.; Castellanos, A.; Elorza-Vidal, X.; Soto, D.; Gasull, X.; Lukacs, G.L.; Estévez, R. Leukoencephalopathy-causing CLCN2 mutations are associated with impaired Cl⁻ channel function and trafficking. *J. Physiol.* **2017**, *595*, 6993–7008. [[CrossRef](#)] [[PubMed](#)]
- Di Bella, D.; Pareyson, D.; Savoirdo, M.; Farina, L.; Ciano, C.; Caldarazzo, S.; Sagnelli, A.; Bonato, S.; Nava, S.; Bresolin, N.; et al. Subclinical leukodystrophy and infertility in a man with a novel homozygous CLCN2 mutation. *Neurology* **2014**, *83*, 1217–1218. [[CrossRef](#)] [[PubMed](#)]
- Hoegg-Beiler, M.B.; Sirisi, S.; Orozco, I.J.; Ferrer, I.; Hohensee, S.; Auberson, M.; Gödde, K.; Vilches, C.; De Heredia, M.L.; Nunes, V.; et al. Disrupting MLC1 and GlialCAM and CIC-2 interactions in leukodystrophy entails glial chloride channel dysfunction. *Nat. Commun.* **2014**, *5*, 3475. [[CrossRef](#)] [[PubMed](#)]
- Goppner, C.; Soria, A.H.; Hoegg-Beiler, M.B.; Jentsch, T.J. Cellular basis of CIC-2 Cl⁻ channel-related brain and testis pathologies. *J. Biol. Chem.* **2021**, *296*, 100074. [[CrossRef](#)] [[PubMed](#)]
- Hoshi, M.; Koshimizu, E.; Miyatake, S.; Matsumoto, N.; Imamura, A. A novel homozygous mutation of CLCN2 in a patient with characteristic brain MRI images—A first case of CLCN2-related leukoencephalopathy in Japan. *Brain Dev.* **2019**, *41*, 101–105. [[CrossRef](#)] [[PubMed](#)]
- Zeydan, B.; Uygungoglu, U.; Altintas, A.; Saip, S.; Siva, A.; Abbink, T.E.M.; van der Knaap, M.S.; Yalcinkaya, C. Identification of 3 Novel Patients with CLCN2-Related Leukoencephalopathy due to CLCN2 Mutations. *Eur. Neurol.* **2017**, *78*, 125–127. [[CrossRef](#)]

19. Giorgio, E.; Vaula, G.; Benna, P.; Buono, N.L.; Eandi, C.M.; Dino, D.; Mancini, C.; Cavalieri, S.; Di Gregorio, E.; Pozzi, E.; et al. A novel homozygous change of CLCN2 (p.His590Pro) is associated with a subclinical form of leukoencephalopathy with ataxia (LKPAT). *J. Neurol. Neurosurg. Psychiatry* **2017**, *88*, 894–896. [[CrossRef](#)]
20. Fu, S.J.; Hu, M.C.; Peng, Y.J.; Fang, H.Y.; Hsiao, C.T.; Chen, T.Y.; Jeng, C.J.; Tang, C.Y. CUL4-DDB1-CRBN E3 Ubiquitin Ligase Regulates Proteostasis of ClC-2 Chloride Channels: Implication for Aldosteronism and Leukodystrophy. *Cells* **2020**, *9*, 1332. [[CrossRef](#)]
21. Balch, W.E.; Morimoto, R.I.; Dillin, A.; Kelly, J.W. Adapting proteostasis for disease intervention. *Science* **2008**, *319*, 916–919. [[CrossRef](#)]
22. Labbadia, J.; Morimoto, R.I. The biology of proteostasis in aging and disease. *Annu. Rev. Biochem.* **2015**, *84*, 435–464. [[CrossRef](#)]
23. Bagola, K.; Mehnert, M.; Jarosch, E.; Sommer, T. Protein dislocation from the ER. *Biochim. Biophys. Acta* **2011**, *1808*, 925–936. [[CrossRef](#)]
24. Vembar, S.S.; Brodsky, J.L. One step at a time: Endoplasmic reticulum-associated degradation. *Nat. Rev. Mol. Cell Biol.* **2008**, *9*, 944–957. [[CrossRef](#)]
25. Guerriero, C.J.; Brodsky, J.L. The delicate balance between secreted protein folding and endoplasmic reticulum-associated degradation in human physiology. *Physiol. Rev.* **2012**, *92*, 537–576. [[CrossRef](#)]
26. Claessen, J.H.; Kundrat, L.; Ploegh, H.L. Protein quality control in the ER: Balancing the ubiquitin checkbook. *Trends Cell Biol.* **2012**, *22*, 22–32. [[CrossRef](#)] [[PubMed](#)]
27. Kim, Y.E.; Hipp, M.S.; Bracher, A.; Hayer-Hartl, M.; Hartl, F.U. Molecular chaperone functions in protein folding and proteostasis. *Annu. Rev. Biochem.* **2013**, *82*, 323–355. [[CrossRef](#)]
28. Houck, S.A.; Cyr, D.M. Mechanisms for quality control of misfolded transmembrane proteins. *Biochim. Biophys. Acta* **2011**, *1818*, 1108–1114. [[CrossRef](#)] [[PubMed](#)]
29. Hebert, D.N.; Molinari, M. In and out of the ER: Protein folding, quality control, degradation, and related human diseases. *Physiol. Rev.* **2007**, *87*, 1377–1408. [[CrossRef](#)] [[PubMed](#)]
30. Wang, X.; Venable, J.; LaPointe, P.; Hutt, D.M.; Koulov, A.V.; Coppinger, J.; Gurkan, C.; Kellner, W.; Matteson, J.; Plutner, H.; et al. Hsp90 cochaperone Aha1 downregulation rescues misfolding of CFTR in cystic fibrosis. *Cell* **2006**, *127*, 803–815.
31. Banasavadi-Siddegowda, Y.K.; Mai, J.; Fan, Y.; Bhattacharya, S.; Giovannucci, D.R.; Sanchez, E.R.; Fischer, G.; Wang, X. FKBP38 peptidylprolyl isomerase promotes the folding of cystic fibrosis transmembrane conductance regulator in the endoplasmic reticulum. *J. Biol. Chem.* **2011**, *286*, 43071–43080. [[CrossRef](#)] [[PubMed](#)]
32. Hutt, D.M.; Roth, D.M.; Chalfant, M.A.; Youker, R.T.; Matteson, J.; Brodsky, J.L.; Balch, W.E. FK506 binding protein 8 peptidylprolyl isomerase activity manages a late stage of cystic fibrosis transmembrane conductance regulator (CFTR) folding and stability. *J. Biol. Chem.* **2012**, *287*, 21914–21925. [[CrossRef](#)] [[PubMed](#)]
33. Koulov, A.V.; LaPointe, P.; Lu, B.; Razvi, A.; Coppinger, J.; Dong, M.-Q.; Matteson, J.; Laister, R.; Arrowsmith, C.; Yates, J.R.; et al. Biological and structural basis for Aha1 regulation of Hsp90 ATPase activity in maintaining proteostasis in the human disease cystic fibrosis. *Mol. Biol. Cell* **2010**, *21*, 871–884.
34. Peng, Y.J.; Huang, J.J.; Wu, H.H.; Hsieh, H.Y.; Wu, C.Y.; Chen, S.C.; Chen, T.Y.; Tang, C.Y. Regulation of CLC-1 chloride channel biosynthesis by FKBP8 and Hsp90beta. *Sci. Rep.* **2016**, *6*, 32444. [[CrossRef](#)] [[PubMed](#)]
35. Hinzpeter, A.; Lipecka, J.; Brouillard, F.; Baudoin-Legros, M.; Dadlez, M.; Edelman, A.; Fritsch, J. Association between Hsp90 and the ClC-2 chloride channel upregulates channel function. *Am. J. Physiol. Cell Physiol.* **2006**, *290*, C45–C56. [[CrossRef](#)]
36. Taipale, M.; Jarosz, D.F.; Lindquist, S. HSP90 at the hub of protein homeostasis: Emerging mechanistic insights. *Nat. Rev. Mol. Cell Biol.* **2010**, *11*, 515–528. [[CrossRef](#)]
37. Shirane, M.; Nakayama, K.I. Inherent calcineurin inhibitor FKBP38 targets Bcl-2 to mitochondria and inhibits apoptosis. *Nat. Cell Biol.* **2003**, *5*, 28–37. [[CrossRef](#)] [[PubMed](#)]
38. Okamoto, T.; Nishimura, Y.; Ichimura, T.; Suzuki, K.; Miyamura, T.; Suzuki, T.; Moriishi, K.; Matsuura, Y. Hepatitis C virus RNA replication is regulated by FKBP8 and Hsp90. *EMBO J.* **2006**, *25*, 5015–5025. [[CrossRef](#)]
39. Rahman, N.A.; Huhtaniemi, I.T. Testicular cell lines. *Mol. Cell Endocrinol.* **2004**, *228*, 53–65. [[CrossRef](#)]
40. Zirkin, B.R.; Papadopoulos, V. Leydig cells: Formation, function, and regulation. *Biol. Reprod.* **2018**, *99*, 101–111. [[CrossRef](#)]
41. Samant, R.S.; Clarke, P.A.; Workman, P. E3 ubiquitin ligase Cullin-5 modulates multiple molecular and cellular responses to heat shock protein 90 inhibition in human cancer cells. *Proc. Natl. Acad. Sci. USA* **2014**, *111*, 6834–6839. [[CrossRef](#)]
42. Ehrlich, E.S.; Wang, T.; Luo, K.; Xiao, Z.; Niewiadomska, A.M.; Martinez, T.; Xu, W.; Neckers, L.; Yu, X.-F. Regulation of Hsp90 client proteins by a Cullin5-RING E3 ubiquitin ligase. *Proc. Natl. Acad. Sci. USA* **2009**, *106*, 20330–20335. [[CrossRef](#)] [[PubMed](#)]
43. Wang, Z.; Hou, Y.; Guo, X.; van der Voet, M.; Boxem, M.; Dixon, J.E.; Chisholm, A.D.; Jin, Y. The EBAX-type Cullin-RING E3 ligase and Hsp90 guard the protein quality of the SAX-3/Robo receptor in developing neurons. *Neuron* **2013**, *79*, 903–916. [[CrossRef](#)]
44. Taipale, M.; Krykbaeva, I.; Koeva, M.; Kayatekin, C.; Westover, K.D.; Karras, G.I.; Lindquist, S. Quantitative analysis of HSP90-client interactions reveals principles of substrate recognition. *Cell* **2012**, *150*, 987–1001. [[CrossRef](#)] [[PubMed](#)]
45. Samant, R.S.; Clarke, P.A.; Workman, P. The expanding proteome of the molecular chaperone HSP90. *Cell Cycle* **2012**, *11*, 1301–1308. [[CrossRef](#)] [[PubMed](#)]
46. Sharma, K.; Vabulas, R.M.; Macek, B.; Pinkert, S.; Cox, J.; Mann, M.; Hartl, F.U. Quantitative proteomics reveals that Hsp90 inhibition preferentially targets kinases and the DNA damage response. *Mol. Cell Proteom.* **2012**, *11*, M111.014654. [[CrossRef](#)] [[PubMed](#)]

47. Wu, Z.; Moghaddas Gholami, A.; Kuster, B. Systematic identification of the HSP90 candidate regulated proteome. *Mol. Cell Proteom.* **2012**, *11*, M111.016675. [[CrossRef](#)] [[PubMed](#)]
48. Powers, M.V.; Workman, P. Targeting of multiple signalling pathways by heat shock protein 90 molecular chaperone inhibitors. *Endocr. Relat. Cancer* **2006**, *13* (Suppl. 1), S125–S135. [[CrossRef](#)]
49. Chiosis, G.; Rodina, A.; Moulick, K. Emerging Hsp90 inhibitors: From discovery to clinic. *Anticancer Agents Med. Chem.* **2006**, *6*, 1–8. [[CrossRef](#)]
50. Jeng, C.J.; Fu, S.J.; You, C.Y.; Peng, Y.J.; Hsiao, C.T.; Chen, T.Y.; Tang, C.Y. Defective Gating and Proteostasis of Human CLC-1 Chloride Channel: Molecular Pathophysiology of Myotonia Congenita. *Front. Neurol.* **2020**, *11*, 76. [[CrossRef](#)]
51. Chen, T.Y. Structure and function of clc channels. *Annu. Rev. Physiol.* **2005**, *67*, 809–839. [[CrossRef](#)]
52. Jentsch, T.J.; Poet, M.; Fuhrmann, J.C.; Zdebik, A.A. Physiological functions of CLC Cl⁻ channels gleaned from human genetic disease and mouse models. *Annu. Rev. Physiol.* **2005**, *67*, 779–807. [[CrossRef](#)] [[PubMed](#)]
53. Chen, Y.A.; Peng, Y.J.; Hu, M.C.; Huang, J.J.; Chien, Y.C.; Wu, J.T.; Chen, T.Y.; Tang, C.Y. The Cullin 4A/B-DDB1-Cereblon E3 Ubiquitin Ligase Complex Mediates the Degradation of CLC-1 Chloride Channels. *Sci. Rep.* **2015**, *5*, 10667. [[CrossRef](#)] [[PubMed](#)]
54. Stricher, F.; Macri, C.; Ruff, M.; Muller, S. HSPA8/HSC70 chaperone protein: Structure, function, and chemical targeting. *Autophagy* **2013**, *9*, 1937–1954. [[CrossRef](#)] [[PubMed](#)]
55. Liu, T.; Daniels, C.K.; Cao, S. Comprehensive review on the HSC70 functions, interactions with related molecules and involvement in clinical diseases and therapeutic potential. *Pharmacol. Ther.* **2012**, *136*, 354–374. [[CrossRef](#)] [[PubMed](#)]
56. Young, J.C. The role of the cytosolic HSP70 chaperone system in diseases caused by misfolding and aberrant trafficking of ion channels. *Dis. Model. Mech.* **2014**, *7*, 319–329. [[CrossRef](#)] [[PubMed](#)]
57. Defranco, D.B. Role of molecular chaperones in subnuclear trafficking of glucocorticoid receptors. *Kidney Int.* **2000**, *57*, 1241–1249. [[CrossRef](#)]
58. Picard, D. Chaperoning steroid hormone action. *Trends Endocrinol. Metab.* **2006**, *17*, 229–235. [[CrossRef](#)]
59. Cato, L.; Neeb, A.; Brown, M.; Cato, A.C. Control of steroid receptor dynamics and function by genomic actions of the cochaperones p23 and Bag-1L. *Nucl. Recept. Signal.* **2014**, *12*, e005. [[CrossRef](#)]
60. Peng, Y.J.; Lee, Y.C.; Fu, S.J.; Chien, Y.C.; Liao, Y.F.; Chen, T.Y.; Jeng, C.J.; Tang, C.Y. FKBP8 Enhances Protein Stability of the CLC-1 Chloride Channel at the Plasma Membrane. *Int. J. Mol. Sci.* **2018**, *19*, 3783. [[CrossRef](#)]
61. Okiyoneda, T.; Barriere, H.; Bagdany, M.; Rabeh, W.M.; Du, K.; Hohfeld, J.; Young, J.C.; Lukacs, G.L. Peripheral protein quality control removes unfolded CFTR from the plasma membrane. *Science* **2010**, *329*, 805–810. [[CrossRef](#)]
62. Pillai, R.N.; Ramalingam, S.S. Heat shock protein 90 inhibitors in non-small-cell lung cancer. *Curr. Opin. Oncol.* **2014**, *26*, 159–164. [[CrossRef](#)]
63. Waza, M.; Adachi, H.; Katsuno, M.; Minamiyama, M.; Sang, C.; Tanaka, F.; Inukai, A.; Doyu, M.; Sobue, G. 17-AAG, an Hsp90 inhibitor, ameliorates polyglutamine-mediated motor neuron degeneration. *Nat. Med.* **2005**, *11*, 1088–1095.
64. Fujikake, N.; Nagai, Y.; Popiel, H.A.; Okamoto, Y.; Yamaguchi, M.; Toda, T. Heat shock transcription factor 1-activating compounds suppress polyglutamine-induced neurodegeneration through induction of multiple molecular chaperones. *J. Biol. Chem.* **2008**, *283*, 26188–26197. [[CrossRef](#)] [[PubMed](#)]
65. Soucy, T.A.; Dick, L.R.; Smith, P.G.; Milhollen, M.A.; Brownell, J.E. The NEDD8 Conjugation Pathway and Its Relevance in Cancer Biology and Therapy. *Genes Cancer* **2010**, *1*, 708–716. [[CrossRef](#)] [[PubMed](#)]
66. McMillin, D.W.; Jacobs, H.M.; Delmore, J.E.; Buon, L.; Hunter, Z.R.; Monrose, V.; Yu, J.; Smith, P.G.; Richardson, P.G.; Anderson, K.C.; et al. Molecular and cellular effects of NEDD8-activating enzyme inhibition in myeloma. *Mol. Cancer Ther.* **2012**, *11*, 942–951. [[CrossRef](#)] [[PubMed](#)]
67. Tanaka, T.; Nakatani, T.; Kamitani, T. Inhibition of NEDD8-conjugation pathway by novel molecules: Potential approaches to anticancer therapy. *Mol. Oncol.* **2012**, *6*, 267–275. [[CrossRef](#)]
68. Brownell, J.E.; Sintchak, M.D.; Gavin, J.M.; Liao, H.; Bruzzese, F.J.; Bump, N.J.; Soucy, T.A.; Milhollen, M.A.; Yang, X.; Burkhardt, A.L.; et al. Substrate-assisted inhibition of ubiquitin-like protein-activating enzymes: The NEDD8 E1 inhibitor MLN4924 forms a NEDD8-AMP mimetic in situ. *Mol. Cell* **2010**, *37*, 102–111. [[CrossRef](#)] [[PubMed](#)]
69. Soucy, T.A.; Smith, P.G.; Milhollen, M.A.; Berger, A.J.; Gavin, J.M.; Adhikari, S.; Brownell, J.E.; Burke, K.E.; Cardin, D.P.; Critchley, S.; et al. An inhibitor of NEDD8-activating enzyme as a new approach to treat cancer. *Nature* **2009**, *458*, 732–736. [[CrossRef](#)] [[PubMed](#)]